A Model for Battery Lifetime Analysis for Organizing Applications on a Pocket Computer

Daler Rakhmatov, Sarma Vrudhula, and Deborah A. Wallach

Abstract— **A battery-powered portable electronic system shuts down once the battery is discharged; therefore, it is important to take the battery behavior into account. A system designer needs an adequate high-level battery model to make battery-aware decisions targeting the maximization of the system's on-line lifetime. We propose such a model: it not only allows a designer to analytically predict the battery time-to-failure for a given load, but also provides a cost metric for an optimization algorithm that aims at lifetime maximization. Our model also allows for a tradeoff between the accuracy and the amount of computation performed. The quality of the proposed model is evaluated using typical pocket computer applications and a detailed low-level simulation of a lithium-ion electrochemical cell. In addition, we verify the proposed model against actual measurements taken on a real lithium-ion battery.**

Keywords— **analysis, low-power-design, performance-tradeoffs, system-level, batteries.**

I. Introduction

Electrical energy in portable systems is commonly supplied by electrochemical batteries, converting chemical energy into electrical energy. The battery capacity is finite, and the time when the battery becomes fully discharged is the lifetime, or *time-to-failure*, of the battery. Once the battery is exhausted the system shuts down; therefore, maximizing the battery time-to-failure is an important problem. Our goal is to develop an analytical model of a generic battery that can be used for estimation and optimization of its time-to-failure under various load conditions.

A system designer can use such a model to evaluate system load alternatives and select one that is the best from a battery perspective. For example, given a set of tasks one can decide on the task schedule and task execution parameters, such as the operating voltage and the clock frequency, so that the battery drain is minimized. Moreover, one can take advantage of the charge *recovery* effects observed during rest periods. These off-line periods can be scheduled with the goal of maximizing system's on-line lifetime. An analytical relationship between the load and the battery time-to-failure can serve as a basis for battery-driven design automation.

Modeling of batteries is difficult due to nonlinearities of charge delivery, which are especially pronounced when the load varies with time. In this paper, "load" refers to the discharge current drawn from the battery. The lifetime L under a *constant* load can be predicted based on empirical relationship due to Peukert [1]: $a = I^b L$, where I is the current, and a and b are appropriate coefficients. This power-law relationship does not hold for a *variable* load (the current is changing over time) when the average current does not adequately represent the battery discharge conditions. According to Peukert's law, all load profiles with the same average would result in the same time-to-failure. This conclusion is not supported by experimental data: our results described later show that for two such profiles the time-to-failure difference can exceed 20%.

We propose a model that provides a more accurate alternative to Peukert's relationship for the constant load case and also works very well for time-varying loads. Our approach also permits a trade-off between the accuracy and the amount of computation performed. Moreover, the proposed relationship is *derived* based on the physical principles of the battery operation.

This paper is organized as follows. Section II provides a brief summary of the recent work on battery modeling. In Section III we derive the model, and in Section IV we estimate model parameters and examine the behavior of the model under constant and time-varying discharge profiles. Section V describes how to estimate the battery lifetime applying the proposed model, and Section VI concludes the paper.

II. Related Work

Battery modeling can be approached in two ways, depending on the level of abstraction. For a battery designer, it is important to know the battery behavior at the *microscopic* scale: an appropriate model should allow for a detailed low-level analysis of the main physical processes taking place inside a complex electrochemical system. However, for a battery user, it is important to know the battery behavior at the *macroscopic* scale. Therefore, a user-level model should only capture the gross characteristics of the battery behavior. Key battery-related issues faced by battery users designing portable electronics, are outlined in [2], [3], [4]. From the design automation perspective, a high-level model is preferable since it is significantly faster than a microscopic model.

The low-level approach relies on a numerical simulation of partial differential equations (PDE) that govern electrochemical processes taking place inside the battery [5], [6]. Consequently, such simulators are computationally intensive and slow. However, they are extremely helpful in extensive studies of the battery systems. (In fact, we used such a simulator to generate experimental data for evaluat-

Daler Rakhmatov and Sarma Vrudhula are with the Center for Low Power Electronics, ECE Department, University of Arizona, 1230 E. Speedway Blvd., Tucson, AZ 85721. E-mail: sarma@ece.arizona.edu.

Deborah A. Wallach is with the Western Research Laboratory, Hewlett-Packard Research Laboratories, 1501 Page Mill Rd. M/S 1251, Palo Alto, CA 94304. E-mail: Deborah.Wallach@hp.com.

ing the quality of our model.) The high-level approach can be based on either simulation of an equivalent representation of a battery [7], [8], [9], or some analytical expression describing how load conditions affect battery performance [3], [10], [11].

The high-level simulation-based models reported in the literature are a PSPICE equivalent circuit [7], a discrete-time VHDL model [8], and a stochastic chain [9]. In terms of the prediction accuracy, the most successful simulation-based approach is due to [9]: it is a Markov chain of the battery charge states with the forward transitions corresponding to discharge, and backward transitions corresponding to recovery. The load is expressed as a random demand on charge units. If, in a given time slot, some number of charge units are "discharged", then an appropriate forward transition takes place (a loss of some charge). If no charge units are demanded, an appropriate backward transition takes place (a recovery of some charge). The experimental results showed accurate lifetime predictions and fast computation times with comparison to the low-level PDE model. This model accounts for both charge delivery nonlinearity and charge recovery effects. However, as with any simulation-based model, a user is expected to specify a large set of model parameters as well as be tolerant of potentially long simulation times.

Next, we briefly outline the referenced work on analytical modeling [3], [10], [11]. The authors of [10] consider special cases of the discharge process (such as diffusion-limited, reaction-limited, and ohmically limited cases) and obtain relationships between the discharge rate and the battery capacity. This work provides valuable information to battery designers, but it is of limited use for battery users. In [3] the authors introduce an efficiency factor to account for charge delivery nonlinearity. They consider two arbitrary approximations for the dependency of this factor on the load: linear and quadratic. Experiments using PSPICE simulations were used to show that the authors' analysis was consistent with a PSPICE model. Unfortunately, the presented data did not demonstrate adequate accuracy of the proposed model. The authors of [11] took a statistical approach. They obtained the battery voltage-time measurement data from several constant-load tests. Fitting of the voltage-time curves into a Weibull model showed a good approximation. Then, a relatively successful attempt was made to model the battery behavior over a range of constant loads; however, time-varying discharge was not considered at all.

Our effort aims at the development of a high-level analytical model based on simplified low-level analysis. We represent the real battery by an equivalent battery, and derive an analytical expression from the physical laws. As with Peukert's law, there are only two unknown parameters which can be estimated using the results of several constant-load tests. Our approach offers the following advantages over previously reported research. First, due to low-level analysis the proposed model is physically justified, which results in its high accuracy and robustness. Second, the analytical nature of the proposed model allows one to utilize it as a cost function for lifetime optimizations. Third, the proposed model is computationally faster and easier to characterize than simulation-based models.

III. Model Description

Every battery has a positive electrode, or *cathode*, and a negative electrode, or *anode*, which are separated by an *electrolyte*. During battery discharge, the anode releases electrons to an external circuit, and the cathode accepts electrons from the circuit. Thus, a loss of electrons (oxidation) at the anode is coupled with the gain of electrons (reduction) at the cathode. During battery charge, the chemical processes are reversed.

Next, we present our view of the battery operation during discharge. It is important to note that we treat the battery electrochemical phenomena at a high level of abstraction. The proposed model is an *equivalent* battery that serves as an approximation of a real battery. As a result, the model is of relatively low complexity while capturing the main characteristics of battery behavior.

We assume that reduction at the anode and oxidation at the cathode are negligible. The electrode reaction, involving ν electrons, oxidized species O, and reduced species R, can be represented as follows [12]:

$$\begin{array}{ll} O + \nu^- \rightarrow R & (cathode), \\ R \rightarrow O + \nu^- & (anode). \end{array} \tag{1}$$

At the cathode, species O accept ν electrons to form species R. Similarly at the anode, species R release ν electrons to form species O. In equilibrium (no load), these electroactive species are uniformly distributed in the electrolyte. Once the external flow of electrons is established, the electrochemical reaction results in reduction of the number of species near the electrode. Thus, a non-zero concentration gradient is created across the electrolyte, and the laws of diffusion apply. If a load is switched off, then the concentration near the electrode surface will start to increase, or *recover*, due to diffusion, and eventually, the concentration gradient will become zero again. In other words, electroactive species will become uniformly distributed in the electrolyte; however, their concentration level will be smaller than the initial value.

Once the concentration of O near the cathode drops below a certain level, the cathode reaction can no longer be sustained. Similarly, once the concentration of R near the anode drops below a certain level, the anode reaction can no longer be sustained. We assume that the cathode and the anode are symmetrical, i.e., O and R behave in the same way. Such an assumption simplifies analysis without impairing the lifetime prediction accuracy, as demonstrated by our experimental results. The time L when the reaction can no longer take place at the electrode surface is the time-to-failure in question.

Our analysis is based on the case of one-dimensional diffusion in a finite region of some length w. Let $C(x,t)$ denote the concentration of species at time $t \in [0, L]$ at distance $x \in [0, w]$ from the electrode. We are interested in the concentration values at the electrode surface ($x = 0$). Let

the initial concentration be C^*, and let $\rho(t) = 1 - \frac{C(0,t)}{C^*}$. When $C(0,t)$ drops below the cutoff level C_{cutoff} at time $t = L$, the value of $\rho(L)$ crosses over the corresponding threshold $(1 - \frac{C_{cutoff}}{C^*})$. In order to compute the time-to-failure L, we need to find an analytical expression for $\rho(t)$.

The following two *Fick's laws* describe concentration behavior due to one-dimensional diffusion [12]:

$$-J(x,t) = D\frac{\partial C(x,t)}{\partial x}, \tag{2}$$

$$\frac{\partial C(x,t)}{\partial t} = D\frac{\partial^2 C(x,t)}{\partial x^2}. \tag{3}$$

$J(x,t)$ denotes the flux of species at time t at distance x, and D denotes the diffusion coefficient. In accordance with *Faraday's law*, the flux at the electrode surface ($x = 0$) is proportional to the current $i(t)$ (the external load applied) [12]. The flux at the other boundary of the diffusion region ($x = w$) is zero. Therefore, the following two boundary conditions apply:

$$\frac{i(t)}{\nu FA} = D\frac{\partial C(x,t)}{\partial x}\bigg|_{x=0}, \tag{4}$$

$$0 = D\frac{\partial C(x,t)}{\partial x}\bigg|_{x=w}. \tag{5}$$

In equation (4), A is the area of the electrode, and F denotes Faraday's constant. It is possible to obtain an analytical solution for these pairs of partial differential equations and boundary conditions. Derivation of the solution is presented in the appendix. The final result is as follows:

$$\rho(t) = \frac{1}{\nu FAwC^*}\Big[\int_0^t i(\tau)\, d\tau + 2\sum_{m=1}^{\infty}\int_0^t i(\tau)\, e^{-\frac{\pi^2 D(t-\tau)m^2}{w^2}}\, d\tau\Big]. \tag{6}$$

Let $\beta = \frac{\pi\sqrt{D}}{w}$ and $\alpha = \nu FAwC^*\rho(L)$. Then, one obtains the following general expression relating the load, the time-to-failure, and the two battery parameters α and β:

$$\boxed{\alpha = \int_0^{\mathbf{L}} \mathbf{i}(\tau)\, \mathbf{d}\tau + \mathbf{2}\sum_{\mathbf{m=1}}^{\infty}\int_0^{\mathbf{L}} \mathbf{i}(\tau)\, \mathbf{e}^{-\beta^2\mathbf{m}^2(\mathbf{L}-\tau)}\, \mathbf{d}\tau.} \tag{7}$$

A. Special Case: Constant Load

For the special case of the constant discharge rate, let $i(t) = I$. The constant I can be brought out of the integrals in equation (7), and we obtain [13]:

$$\boxed{\alpha = \mathbf{IL}\Big[\mathbf{1} + \mathbf{2}\sum_{\mathbf{m=1}}^{\infty}\frac{\mathbf{1} - \mathbf{e}^{-\beta^2\mathbf{m}^2\mathbf{L}}}{\beta^2\mathbf{m}^2\mathbf{L}}\Big].} \tag{8}$$

The magnitude of the sum terms in equation (8) diminish very rapidly. Figure 1 shows the plots of the sum truncated after the first 10 terms and after the first 100000 terms, as a function of $\beta^2 L$ (the factor of index m) ranging from 1 to 100. The first 10 terms provide a good approximation to the entire sum for $\beta^2 L \geq 1$. Our lifetime calculations involving 100000 terms have resulted in negligible

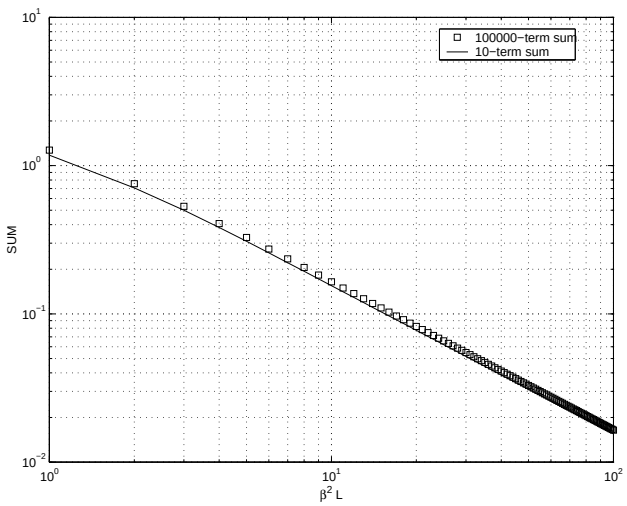

Fig. 1. Approximation for Infinite Sum in Equation 8.

improvement in accuracy, while considerably slowing down the computation process.

Thus,

$$\alpha \approx I\Big[L + 2\sum_{m=1}^{10}\frac{1 - e^{-\beta^2 m^2 L}}{\beta^2 m^2}\Big]. \tag{9}$$

For the constant load case, Peukert's law states that

$$a = I^b L. \tag{10}$$

Note that equation (10) is an empirical relationship, without any physical justification. As a result, its possible extensions to the variable load case are inherently heuristic.

B. General Case: Variable Load

We approximate the time-varying discharge rate by a piece-wise constant load: Figure 2 shows an example of such an approximation. Let the step function be denoted by $U(t)$. Then, the variable load $i(t)$, approximated in the interval $[0,t]$ by an N-step staircase function is expressed as

$$i(t) \approx \sum_{k=0}^{N-1} I_k[U(t - t_k) - U(t - t_{k+1})]. \tag{11}$$

After substitution of $i(t)$ into equation (7) and integrating the sum term by term we obtain:

$$\alpha \approx \sum_{k=0}^{N-1} I_k\Big[\int_{t_k}^{t_{k+1}} d\tau + 2\sum_{m=1}^{\infty}\int_{t_k}^{t_{k+1}} e^{-\beta^2 m^2 (L-\tau)}\, d\tau\Big]. \tag{12}$$

Then,

$$\boxed{\alpha \approx \sum_{\mathbf{k=0}}^{\mathbf{N-1}} \mathbf{I_k F(L, t_k, t_{k+1}, \beta)},} \tag{13}$$

where

$$F(L, t_k, t_{k+1}, \beta) = t_{k+1} - t_k + 2\sum_{m=1}^{\infty}\frac{e^{-\beta^2 m^2 (L - t_{k+1})} - e^{-\beta^2 m^2 (L - t_k)}}{\beta^2 m^2}. \tag{14}$$

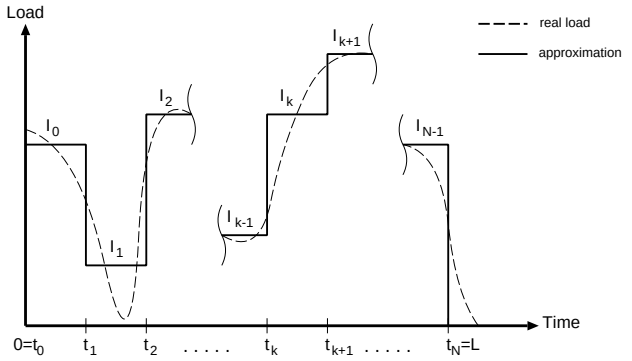

Fig. 2. Staircase Approximation of Variable Load.

When computing $F(L, t_k, t_{k+1}, \beta)$, we use only the first ten terms of the series. For $N = 1$, equation (13) reduces to the special case described by equation (9). It is important to note that $t_0 = 0$ and $t_N = L$.

A straightforward extension of Peukert's equation to the variable load case is to average discharge currents over the interval $[0, L]$. Since the load average depends on L, solving this equation for L becomes difficult. Such generalization of Peukert's law is expressed as

$$a \approx \left[\frac{\sum_{k=0}^{N-1} I_k(t_{k+1} - t_k)}{L}\right]^b L. \qquad (15)$$

Note that the unknown L appears inside the N-term sum as well, since $t_N = L$. For $N = 1$, equation (15) reduces to equation (10).

C. Parameter Estimation

Recall that our model is an abstraction of a real battery. In order for our model to perform adequately, we need to choose the parameters α and β appropriately, so that predicted and observed lifetimes match closely. Thus, before one can use the proposed model, the parameters α and β need to be estimated from experimental data for the modeled battery. Simple experiments with constant loads are *sufficient* for estimation purposes, and one can utilize equation (9).

For a given battery under a given load, the battery voltage changes over time from the open-circuit value V_{oc} to some cutoff value V_{cutoff}. The *observed* lifetime is defined as the time when the battery voltage reaches V_{cutoff}. The *predicted* lifetime is defined as the time value for which the equality (9) holds. For a given set of M constant loads $\{I_{(1)}, I_{(2)}, ..., I_{(M)}\}$, the corresponding set of M observed lifetimes is $\{L_{(1)}, L_{(2)}, ..., L_{(M)}\}$. The objective is to find α and β such that the predicted lifetimes match the observed lifetimes as closely as possible. However, this objective is hard to pursue directly, since equation (9) is hard to solve for the unknown L. Alternatively, one can estimate parameters by fitting the load values for a given set of observed lifetimes. Let $\hat{I}_{(k)}$ denote the fitted value of $I_{(k)}$. According to equation (9),

$$\hat{I}_{(k)} \approx \frac{\alpha}{L_{(k)} + 2\sum_{m=1}^{10} \frac{1 - e^{-\beta^2 m^2 L_{(k)}}}{\beta^2 m^2}} \qquad (16)$$

The objective now is to find α and β such that $\hat{I}_{(k)}$ matches $I_{(k)}$ as closely as possible for all $1 \le k \le M$. One can employ a standard least-squares estimator for this purpose: the model parameters are selected so that $\sum_{k=1}^{M} |\hat{I}_{(k)} - I_{(k)}|^2$ is minimized.

IV. Experimental Results

The low-level simulator DUALFOIL [5], [6] was used to simulate a rechargeable lithium-ion battery. DUALFOIL numerically solves partial differential equations of electrochemical processes. A user must supply over 50 parameters in order to specify a simulated battery. As a battery load, we used realistic power consumption data observed during pocket computer operation [14].

A. Simulated Battery

Viredaz and Wallach [14] performed an extensive power evaluation of the Compaq Itsy pocket computer, a research platform based on the StrongARM SA-1100 processor. Power consumption for different applications as well as corresponding battery lifetimes were measured. Itsy features a precision sense resistor in series with the battery. The voltage drop across this resistor as well as the Itsy's input voltage were measured by two external multimeters. The experiments were automatically controlled by a host computer connected to Itsy and the multimeters via a serial link. From the results of these studies described in [14], we selected ten Itsy loads, whose measured lifetimes ranged from 2 hours to 9 days. These loads are summarized in Table I.

TABLE I
Description of Itsy Loads.

Test	Name	Description	P_{ave} mW	I_{ave} mA
T1	MPEG	video, 206MHz	835	222.7
T2	Dictation	speech input, 206Hz	767	204.5
T3	Talk1	speech output, 206MHz	406	108.3
T4	Talk2	speech output, 74MHz	403	107.5
T5	Talk3	speech output, 74MHz (LV)	356	94.9
T6	WAV1	audio, 206MHz	316	84.3
T7	WAV2	audio, 59MHz	283	75.5
T8	Idle1	operating system, 206MHz	105	28.0
T9	Idle2	operating system, 59MHz	73	19.5
T10	SleepDC	sleep with a daughter-card	11	3.0

We assumed that average battery voltage is 3.75 V [14] (to obtain average current values from average power values) and adjusted 30 simulation settings, based on the data from [15]. The open-circuit voltage V_{oc} of the simulated battery was 4.3 V, and the cutoff voltage V_{cutoff} was set to 3.2 V. With these settings, the chosen Itsy loads were simulated using DUALFOIL. The resulting lifetime estimates and the measurements are displayed in Table II and shown graphically in Figure 3. For the range of currents

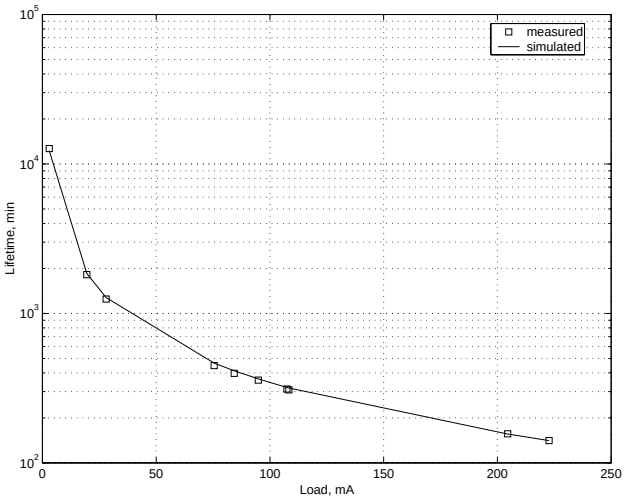

Fig. 3. Measured (Itsy) and Simulated (DUALFOIL) Lifetimes.

considered, the measured and simulated lifetimes matched closely: the average error was 2%, and the maximum error was 4%. Note, however, that the DUALFOIL battery is not intended to represent the Itsy battery, since neither the chemical nor the mechanical structure of the latter is known.

TABLE II
Measured (Itsy) and Simulated (DUALFOIL) Lifetimes.

Test	Measured, min	Simulated, min	Error, %	Error, min
T1	141.0	140.9	0.1	0.1
T2	156.6	156.0	0.4	0.6
T3	307.8	317.2	3.1	9.4
T4	312.0	319.5	2.4	7.5
T5	358.2	365.1	1.9	6.9
T6	397.2	413.7	4.2	16.5
T7	448.2	464.8	3.7	16.6
T8	1248	1278	2.4	30
T9	1818	1852	1.9	34
T10	12690	12285	3.2	405

B. Constant Loads

To cover a sufficient range of currents besides those for T1-T20, twelve additional constant loads were simulated, resulting in the discharge times as low as 1/2 hour. We assumed that Itsy had additional peripheral devices such as a Microdrive hard disk [16] and a WaveLAN wireless card [17]. The Microdrive consumes 66 mW in standby and 825 mW during write/read. The WaveLAN consumes 45 mW in the doze state, 925 mW while receiving, and 1425 mW while transmitting. The twelve additional loads are described in Table III by a 3-letter code. These three letters indicate the state of the Itsy, the Microdrive, and the WaveLAN, respectively. The last load, *Boot*, corresponds to rebooting of Itsy, and we assume that current consumption in this case is approximately 300 mA [18]. The following letter abbreviations are used:

- **Itsy:** I – Idle1, M – MPEG, D – Dictation, T – Talk1, W – WAV1, S – SleepDC
- **Microdrive:** S – standby, A – access

TABLE III
Itsy Load Values with Peripherals.

Test	Name	P_{ave}, mW	I_{ave}, mA
T11	IAT	2355	628.0
T12	IAR	1855	494.7
T13	IST	1596	425.6
T14	ISR	1096	292.3
T15	IAD	996	265.6
T16	MSD	946	252.3
T17	DSD	878	234.1
T18	TSD	517	137.9
T19	WSD	427	113.9
T20	ISD	216	57.6
T21	SSD	122	32.5
T22	Boot	1125	300.0

- **WaveLAN:** D – doze, R – receive, T – transmit

B.1 Model parameters and predictions

Given these thirty-two time-to-failure values, one can estimate the model parameters α and β, as described in the previous section. We used a standard least-squares estimation procedure to fit the data to our model and, for comparison purposes, to Peukert's law. The estimated parameters are as follows:

- $\alpha = 40375$ and $\beta = 0.273$ (our model)
- $a = 37520$ and $b = 1.016$ (Peukert's law)

The lifetime predictions, based on equations (9) and (10) with the estimated coefficients, are shown in Table IV. Both relative ($\Delta\%$) and absolute (Δmin) errors are given. Note that for heavy loads, resulting in a battery failure within six hours, our prediction error was within 5%; whereas, for light loads, yielding lifetimes of more than six hours, our prediction error was between 5% and 10%. Peukert's law exhibits the opposite behavior. It is accurate within 2% for light loads, but it is extremely inaccurate for heavy loads. The maximum error of Peukert's predictions was more than 100%, and in 8 out of 22 tests the error was more than 10%.

C. Variable Loads

In this section we describe twenty-two variable load experiments performed with the DUALFOIL simulator and compare the simulated lifetimes with our predictions. We use equation (13) to compute the time-to-failure L of the battery. For comparison purposes, we also compute the lifetime estimates based on Peukert's law. The purpose of these experiments is to see how robust our model is and how changes in load profiles affect the battery lifetime. The time-to-failure is computed with the accuracy of 0.1 minute. Table V describes the experiments, and Table VII provides profile specifications.

C.1 Variable-load profile specification

In order to specify a load profile we introduce two ordered sets for load values and their timing: $S_I = (I_0, I_1, ..., I_{n-1})$ and $S_t = (t_0, t_1, ..., t_{n-1})$, in accordance with Figure 2. For example, in case C1, $S_I = (628.0, 0, 628.0)$ and $S_t = (0, 19.5, 26.0)$. This means that the battery was discharged

TABLE IV
Lifetime Predictions for Constant Loads.

Simulation		*Our Model*			*Peukert's Law*		
test	min	min	Δ%	Δmin	min	Δ%	Δmin
T1	140.9	139.9	0.1	1.0	154.5	9.7	13.6
T2	156.0	156.0	0.0	0.0	168.4	7.9	12.4
T3	317.2	331.4	4.5	14.2	321.3	1.2	3.8
T4	319.5	334.1	4.6	14.6	323.7	1.3	4.2
T5	365.1	384.0	5.2	18.9	367.5	0.7	2.4
T6	413.7	437.5	5.8	23.8	414.4	0.2	0.7
T7	464.8	493.3	6.1	28.5	463.6	0.3	1.2
T8	1278	1400	9.5	122	1270	0.6	8.0
T9	1852	2029	9.6	177	1834	1.0	18.0
T10	12285	13417	9.2	1132	12288	0.0	3.0
T11	26.0	26.6	2.3	0.6	53.9	107.3	27.9
T12	41.3	41.4	0.2	0.1	68.6	66.1	27.3
T13	54.6	53.9	1.3	0.7	80.0	46.5	25.4
T14	99.5	96.7	2.8	2.8	117.2	17.8	17.7
T15	113.1	110.6	2.2	2.5	129.1	14.1	16.0
T16	120.8	118.6	1.8	2.2	136.1	12.7	15.3
T17	132.7	131.0	1.3	1.7	146.8	10.6	14.1
T18	243.6	251.3	3.2	7.7	251.4	3.2	7.8
T19	300.1	313.0	4.3	12.9	305.3	1.7	5.2
T20	616.3	659.5	7.0	43.2	610.3	1.0	6.0
T21	1101	1201	9.1	100	1092	0.8	9.0
T22	96.0	93.2	2.9	2.8	114.1	18.9	18.1

TABLE V
Variable-Load Profile Description.

Case	Description
C1	IAT-off-IAT
C2	IAR-off-IAR
C3	IST-off-IST
C4	ISR-off-ISR
C5	MPEG-off-MPEG
C6	IAT-off-IAT
C7	IAT-off-IAT
C8	IAT-off-IAT
C9	IAT-off-IAT
C10	Boot-IAT-IAR-MSD-DSD-TSD-WSD-IAD
C11	Boot-WSD-TSD-DSD-MSD-IAR-IAT-IAD
C12	Boot-WSD-TSD-DSD-MSD-IAR-off-Boot-IAT-IAD
C13	Boot-$[$IAT-IAR-MSD-DSD-TSD-WSD$]^5$-IAD
C14	Boot-$[$WSD-TSD-DSD-MSD-IAR-IAT$]^5$-IAD
C15	MPEG-Dictation-Talk1-WAV1-MPEG
C16	WAV1-Talk1-Dictation-MPEG-MPEG
C17	WAV1-Talk1-Dictation-off-MPEG-MPEG
C18	$[$WAV1-Talk1-Dictation-MPEG$]^{10}$-MPEG
C19	$[$WAV2-Talk3-Dictation-MPEG$]^{10}$-MPEG
C20	$[$IAR-IAT$]^{\infty}$
C21	$[$IAR-IAT-ISD$]^{\infty}$
C22	$5.0 + 5.0/min$

at 628 mA for the first 19.5 min and then started again from the 26th minute, while there was no load during the time interval [19.5, 26.0]. The finish time t_n of the last load is set to infinity for each profile.

To avoid repetition for periodic loads, we enclose the first period into square brackets (see cases C13, C14, C18, C19, C20, and C21); the subscript indicates the duration of one period, and the superscript indicates the number of periods. For example, in case C19, $S_I = ([75.5, 94.9, 204.5, 222.7]^{10}, 222.7)$ and $S_t = ([0, 5.0, 10.0, 15.0]^{10}_{20.0}, 200.0)$. This means that ten 20-minute periods were applied before the battery started to discharge at the constant rate of 222.7 mA. Within each period, 75.5 mA was applied for the first 5 min, 94.9 mA for the second 5 min, 204.5 mA for the next 5 min, and 222.7 mA for the last 5 min.

For cases C20 and C21 the number of periods is infinite: the battery time-to-failure determines how many periods were serviced. For the last case C22, the load is increasing from 5.0 mA by 5.0 mA with every minute.

TABLE VI
Lifetime Predictions for Variable Loads.

Simulation		*Our Model*			*Peukert's Law*		
case	min	min	Δ%	Δmin	min	Δ%	Δmin
C1	36.4	36.2	0.5	0.2	60.5	66.2	24.1
C2	57.2	55.8	2.4	1.4	79.1	38.3	21.9
C3	74.2	71.9	3.1	2.3	93.8	26.4	19.6
C4	128.1	124.9	2.5	3.2	142.5	11.2	14.4
C5	178.5	176.7	1.0	1.8	190.2	6.6	11.7
C6	41.5	41.0	1.2	0.5	64.4	55.2	22.9
C7	30.6	30.8	0.7	0.2	56.5	84.6	25.9
C8	37.0	37.4	1.1	0.4	60.5	63.5	23.5
C9	35.4	35.2	0.6	0.2	60.5	70.9	25.1
C10	135.2	132.6	1.9	2.6	148.8	10.1	13.6
C11	108.8	107.4	1.3	1.4	148.8	36.8	40.0
C12	159.0	155.4	2.3	3.6	174.1	9.5	15.1
C13	133.8	131.7	1.6	2.1	148.8	11.2	15.0
C14	132.9	129.7	2.4	3.2	148.8	12.0	15.9
C15	207.6	209.2	0.8	1.6	216.2	4.1	8.6
C16	202.4	200.7	0.8	1.7	216.2	6.8	13.8
C17	253.8	251.2	1.0	2.6	266.7	5.1	12.9
C18	204.6	204.6	0.0	0.0	216.2	5.7	11.6
C19	209.4	208.7	0.3	0.7	221.2	5.6	11.8
C20	31.7	33.2	4.7	1.5	60.5	90.9	28.8
C21	55.9	55.9	0.0	0.0	85.9	53.7	30.0
C22	97.5	94.5	3.1	3.0	117.9	20.9	20.4

C.2 General result

The results of the experiments with the variable loads are shown in Table VI and graphed in Figure 4. The range of lifetimes was from 1/2 hour to 4 hours. Not surprisingly, Peukert's law performed poorly in as many as half of the cases with the error exceeding 20% and reaching 90%. Our model not only correctly captured the *trend* in battery behavior, but also produced results within a 5% error margin. In terms of absolute errors, Peukert's law might be off by as much as 40 min, whereas our model was accurate up to 4 min.

C.3 Recovery effect

The first nine cases C1-C9 are intended to expose the recovery effect. In each case, a continuous load is applied for some period of time, interrupted by a rest period, and switched back on until the battery fails. The lifetime under a continuous (uninterrupted) load is denoted by $L_{original}$ (see Table IV). The lifetime under an interrupted load when there is no recovery is denoted by $L_{unaffected}$, which is equal to the sum of $L_{original}$ and the duration of the rest period. The actual lifetime observed under an interrupted load is denoted by L. These three lifetimes are presented in Table VIII, along with the recovery gain percentage with respect to $L_{original}$ not including the duration of the rest period itself.

In cases C1-C5 the battery was discharged for $0.75L_{original}$ minutes, rested for $0.25L_{original}$ minutes, and

TABLE VII
Simulated Variable-Load Profiles.

Case	Value Set S_I, mA	Timing Set S_t, min
C1	(628.0, 0, 628.0)	(0, 19.5, 26.0)
C2	(494.7, 0, 494.7)	(0, 31.0, 41.3)
C3	(425.6, 0, 425.6)	(0, 41.0, 54.6)
C4	(292.3, 0, 292.3)	(0, 74.6, 99.5)
C5	(222.7, 0, 222.7)	(0, 105.7, 140.9)
C6	(628.0, 0, 628.0)	(0, 19.5, 29.9)
C7	(628.0, 0, 628.0)	(0, 19.5, 22.1)
C8	(628.0, 0, 628.0)	(0, 23.4, 29.9)
C9	(628.0, 0, 628.0)	(0, 15.6, 22.1)
C10	(300.0, 628.0, 494.7, 252.3, 234.1, 137.9, 113.9, 265.6)	(0, 0.5, 5.5, 10.5, 35.5, 60.5, 85.5, 110.5)
C11	(300.0, 113.9, 137.9, 234.1, 252.3, 494.7, 628.0, 265.6)	(0, 0.5, 25.5, 50.5, 75.5,, 100.5, 105.5, 110.5)
C12	(300.0, 113.9, 137.9, 234.1, 252.3, 494.7, 0, 300.0, 628.0, 265.6)	(0, 0.5, 25.5, 50.5, 75.5, 100.5, 105.5, 130.5, 131.0, 136.0)
C13	(300.0, $[628.0, 494.7, 252.3, 234.1, 137.9, 113.9]^5$, 265.6)	(0, $[0.5, 1.5, 2.5, 7.5, 12.5, 17.5]^5_{22.5}$, 110.5)
C14	(300.0, $[113.9, 137.9, 234.1, 252.3, 494.7, 628.0]^5$, 265.6)	(0, $[0.5, 5.5, 10.5, 15.5, 20.5, 21.5]^5_{22.5}$, 110.5)
C15	(222.7, 204.5, 108.3, 84.3, 222.7)	(0, 50.0, 100.0, 150.0, 200.0)
C16	(84.3, 108.3, 204.5, 222.7, 222.7)	(0, 50.0, 100.0, 150.0, 200.0)
C17	(84.3, 108.3, 204.5, 0, 222.7, 222.7)	(0, 50.0, 100.0, 150.0, 200.0, 250.0)
C18	($[84.3, 108.3, 204.5, 222.7]^{10}$, 222.7)	($[0, 5.0, 10.0, 15.0]^{10}_{20.0}$, 200.0)
C19	($[75.5, 94.9, 204.5, 222.7]^{10}$, 222.7)	($[0, 5.0, 10.0, 15.0]^{10}_{20.0}$, 200.0)
C20	($[494.7, 628.0]^{\infty}$)	($[0, 1.0]^{\infty}_{2.0}$)
C21	($[494.7, 628.0, 57.6]^{\infty}$)	($[0, 1.0, 2.0]^{\infty}_{3.0}$)
C22	(5.0, 10.0, 15.0, ...)	(0, 1.0, 2.0, ...)

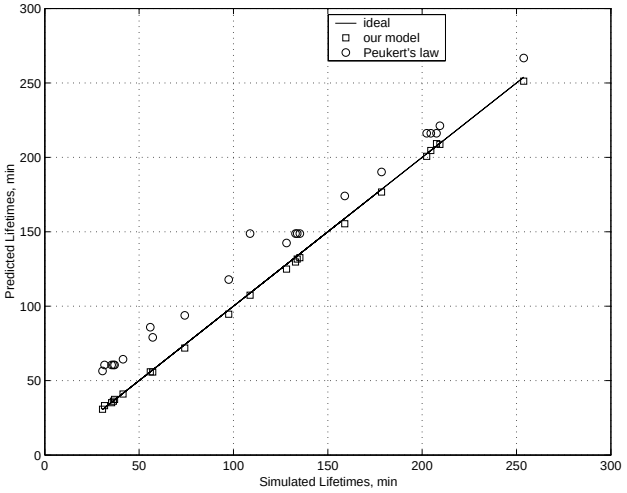

Fig. 4. Predicted vs Simulated Variable-Load Lifetimes.

then continued discharging afterwards. One can see that the higher the load, the greater the recovery effect. For the next cases C6-C9 case C1 was used as a basis. In C6 and C7 the rest period was changed by $0.15L_{original}$ (increased to $0.4L_{original}$ in C6 and decreased to $0.1L_{original}$ in C7), while the start time of the rest period remained unchanged. As expected, the results show that the longer the recovery time, the greater the recovery effect. In C8 and C9 the start time of the rest period was changed by $0.15L_{original}$ (increased to $0.9L_{original}$ in C8 and decreased to $0.6L_{original}$ in C9), while the duration of the rest period remained unchanged. These two cases indicate that the amount of recovery also depends on the depth of discharge.

For heavy periodic loads, the battery can deliver extra charge provided that an idle load is inserted within each

TABLE VIII
Recovery of the DUALFOIL Battery under Interrupted Loads.

Case	$L_{original}$, min	$L_{unaffected}$, min	L, min	Recovery, %
C1	26.0	32.5	36.4	15.0
C2	41.3	51.6	57.2	13.6
C3	54.6	68.2	74.2	11.0
C4	99.5	124.4	128.1	3.7
C5	140.9	176.1	178.5	1.7
C6	26.0	36.4	41.5	19.6
C7	26.0	28.6	30.6	7.7
C8	26.0	32.5	37.0	17.3
C9	26.0	32.5	35.4	11.2

period. Note that recovery is observed when a heavy load is followed by a light load, i.e., the battery still remains on-line.

In case C20, the period was 2 min, and in case C21, the period was extended by 1 min to accommodate the idle load. Note that this idle mode invokes not only a delay penalty but also an energy penalty because the system is not off-line. Nevertheless, in case C21 the battery serviced 18 full periods; while, in case C20 it serviced only 15 full periods.

C.4 Heavy peak-power loading

For cases C10-C14 the peak load is 628.0mA. If it is applied continuously, the DUALFOIL battery "dies" in less than 1/2 hour (see test T11). Note that different load arrangements in a sequence do not change the peak power of the resulting profile; nevertheless, the battery lifetime may still be greatly affected. Next, we describe what may be beneficial for the battery when the peak load is heavy.

On comparing cases C10 and C11, one can observe that

sequencing non-periodic loads in nonincreasing order of their values, if load dependencies allow, results in a better lifetime. In other words, the battery can handle high loads better at the beginning than in at the end of discharge. In both C10 and C11, the first loads are the same, and so are the last loads. However, the remaining loads are arranged in nonincreasing (nondecreasing) order in case C10 (case C11). Note that in C10 the battery lasted more than 20 min past the start time of the last load (110.5 min); whereas, in C11 the battery was exhausted before the last load started. These two cases demonstrate that proper load sequencing can significantly affect lifetime.

It may also be beneficial to convert, if dependencies allow, a non-periodic load into a periodic load, or in other words, "spread out" the load values across the profile. For example, in C14 – a periodic version of C11 – the nondecreasing load sequence between the first and the last loads was distributed across five periods. As a result heavy loads alternated with light loads over time, and lifetime was improved by more than 20 min. However, as cases C13 and C14 indicate, for periodic loads, the nonincreasing ordering within a period does not improve the lifetime considerably.

Inserting rest periods is clearly helpful when the battery is subject to heavy loads. The profile of C12 is similar to C11, except that a rest period of 25 min and the following 0.5-minute *Boot* are inserted before the load of 628.0 mA. This rest period invokes not only a delay penalty of 25.5 min, but also an energy penalty due to rebooting of Itsy. Nevertheless, in C12 Itsy was able to complete more work than in the case of C11: 159.0 – 25.5 = 133.5 min in C12 vs. 108.8 min in C11.

C.5 Light peak-power loading

For cases C15-C19 with the peak load of 222.7 mA, the battery behavior is somewhat stable: the lifetime variations are not significant. As a result, extensions of Peukert's model might work fairly well. Note that the lifetime under the continuous load of 222.7 mA is more than two hours (see test T1).

In case C15, the loads are scheduled in nonincreasing order of their current consumption values, except for the last load, whereas in case C16, the order is nondecreasing. As expected, the lifetime in case C15 is slightly better than the lifetime in case C16, and in both cases the battery continue operating beyond the start time of the last load. Case C18 is a periodic version of case C16, excluding the last load; again, lifetime was slightly improved with comparison to C16. The profile in case C17 contains a 50-minute long rest period; even though there is a slight improvement over case C16, the lifetime increase is too small to justify the 50-minute delay penalty. The case C19 is similar to case C18, except that the WAV1 and Talk1 loads are replaced by the lighter WAV2 and Talk3 loads, respectively. Clearly, such a replacement has a positive effect on the lifetime; however, the improvement was somewhat marginal.

D. Averaging Battery Voltage and Current

For the experiments described in this section, we used loads with coarse-grain timing (0.1-minute timing scale resolution). During each step k (see Figure 2), the discharge current I_k is assumed to be a constant average. A natural question arises about whether this assumption is reasonable. First of all, timing granularity is a *user's choice*. Lower timing granularity yields more accurate load description. One may specify the battery current at each clock cycle, if desired. However, the battery is inherently a very slow device, and averaging the battery current at a frequency of more than 1Hz (1-second timing scale resolution) is not practical [2]. Also, the battery lifetime is usually expressed in terms of minutes and hours. Using the accuracy of 1 s to predict the battery lifetime of several hours requires a large amount of computation, which may often be wasteful since battery parameters fluctuate due to manufacturing lot variations, discharge-recharge cycling effects, and temperature changes. Here, we predict lifetimes with the accuracy of 0.1 min. Again, note that using fractions of a minute instead of seconds or microseconds is specific only to the experimental results, not the proposed model itself: a user can use *any* time scale and a current averaging window of *any* size.

Another issue is related to the battery voltage, which is not involved in equation (13). A user is expected to specify the current $i(t)$ drawn from the battery during application execution. If $i(t)$ is not known directly, one can let $i(t) = P(t)/(\mu V_{ave})$, where μ is the efficiency of the DC-DC converter, $P(t)$ is the power consumption of an application, and V_{ave} is the average battery voltage. Is it acceptable to use a constant average V_{ave} for varying battery voltage? To answer this question we used measurement results for the Itsy battery reported in [19], which are presented in Table IX. The first column shows different types of Itsy applications (see tests T1-T9). Given the average battery power P_{ave} delivered for each application, as shown in the second column, the following experiments were performed. First, the Itsy battery was discharged in a constant-power discharge mode, with the constant power set to P_{ave}. Second, the Itsy battery was discharged in a constant-current mode, with the constant current set equal to $P_{ave}/3.75V$, where 3.75V is the average used for the Itsy battery voltage [14]. The corresponding lifetimes are shown in the third and the fourth columns, respectively. Note that during constant-power discharge, the product of the battery current and the battery voltage is maintained constant. Since the battery voltage is decreasing, the battery current is increasing, i.e., it is not constant. However, during constant-current discharge, the battery current is maintained constant, under the assumption that the battery voltage is constant V_{ave}. As one can see that lifetimes for both cases match closely: the relative error does not exceed 3%. These results suggest battery voltage averaging is an acceptable measure for reducing problem complexity associated with battery lifetime predictions.

TABLE IX
Effect of Battery Voltage Averaging.

Name	P_{ave} mW	$P = const$ L, min	$I = const$ L, min	$Error$ $\Delta\%$	Δmin
MPEG	835	152.4	150.6	1.2	1.8
Dictation	767	167.4	168.0	0.4	0.6
Talk1	406	327.0	321.0	1.8	6.0
Talk2	403	330.6	324.0	2.0	6.6
Talk3	356	376.8	370.8	1.6	6.0
WAV1	316	421.8	415.8	1.4	6.0
WAV2	283	473.4	467.4	1.3	6.0
Idle1	105	1309.8	1284.0	2.0	25.8
Idle2	73	1888.8	1839.6	2.6	49.2

E. Measurement Results

In addition to simulations, we have performed actual measurements on a real 2.2 W-h battery for the constant-current tests T11-T22 and the variable-current profiles C1-C21. Table X presents the results for the constant loads, and Table XI presents the results for the variable loads.

TABLE X
Measured and Predicted Lifetimes for Constant Loads.

Test	Measured, min	Predicted, min	Error, %	Error, min
T11	48.0	48.2	0.4	0.2
T12	62.9	62.7	0.3	0.2
T13	74.6	73.7	1.2	0.9
T14	110.7	109.9	0.7	0.8
T15	118.1	121.4	2.8	3.3
T16	124.8	128.1	2.6	3.3
T17	138.7	138.5	0.1	0.2
T18	240.8	239.0	0.7	1.8
T19	293.5	290.5	1.0	3.0
T20	592.4	579.7	2.1	12.7
T21	1069	1032	3.5	37
T22	105.4	106.9	1.4	1.5

Given the measured lifetimes from Table X and the constant currents from Table III, we obtained the following estimates of the model parameters: $\alpha = 33706$ and $\beta = 0.750$. The second column of Table X shows the predicted lifetimes based on the estimated α and β. One can see that the maximum error does not exceed 4%.

Table XI presents the measured and predicted lifetimes for the cases C1-C21. Note that the maximum error is only 1%. However, this remarkable accuracy can be somewhat misleading. Note that the high value of $\beta = 0.750$ (compare with $\beta = 0.273$ for the DUALFOIL battery) suggests that the tested battery does not exhibit significant nonlinear effects. Consequently, predicting the lifetime of such a well-behaved battery within an acceptable error margin is not difficult. In other words, our model is not exercised in terms of how well it can account for nonlinear effects. Note that the nonlinear component of the proposed model (13) becomes negligible for sufficiently large values of β.

Here, we omit presentation of the lifetime predictions due to Peukert's law. Since the battery under test is well-behaved, the power-law relationship is an adequate model: the maximum prediction errors for constant-load and variable-load tests does not exceed 4%. Nevertheless, note that our model is still superior in terms of precision.

TABLE XI
Measured and Predicted Lifetimes for Variable Loads.

Case	Measured, min	Predicted, min	Error, %	Error, min
C1	54.5	54.7	0.4	0.2
C2	73.3	73.0	0.4	0.3
C3	88.3	87.3	1.1	1.0
C4	136.0	134.8	0.8	1.2
C5	182.7	181.1	0.9	1.6
C6	59.0	58.6	0.8	0.4
C7	51.1	50.8	0.6	0.3
C8	55.0	54.7	0.5	0.3
C9	54.9	54.7	0.4	0.2
C10	142.7	140.8	1.3	1.9
C11	141.4	140.8	0.4	0.6
C12	166.6	165.7	0.5	0.9
C13	141.3	140.8	0.4	0.5
C14	141.8	140.8	0.7	1.0
C15	208.6	206.8	0.9	1.8
C16	207.4	206.7	0.3	0.7
C17	257.6	256.7	0.3	0.9
C18	209.3	206.7	1.2	2.6
C19	213.7	211.7	0.9	2.0
C20	55.0	55.0	0.0	0.0
C21	79.1	79.2	0.1	0.1

Due to weak nonlinearity of the tested battery, charge recovery effects are negligible, as the lifetimes for cases C1-C9 indicate. For example, in case C6, $L_{original}$ is 48.0 min, and the duration of the rest period is 10.4 min, i.e. $L_{unaffected}$ is 58.4 min. Note that the measured lifetime for C6 is 59.0 min, which corresponds to a lifetime improvement of only 1%. For cases C20 and C21, the battery serviced 27 and 26 full periods, respectively. Recall that the DUALFOIL battery lasts longer under C21 than under C20. Since charge recovery of the tested battery is negligible, the energy penalty due to the idle load in C21 is not compensated, which results in the slightly worse lifetime than in case C20. Also, note that in case C12 (case C17), the rest period of 25.0 min (50.0 min) yields no advantage over case C11 (case C16).

As expected for the tested battery, case pairs C10-C11, C13-C14, and C15-C16 demonstrate that the lifetime dependence on load ordering is much weaker than for the DUALFOIL battery. Finally, note that in case C19, reducing power consumption with respect to case C18 results in a 2% extension of the battery lifetime (213.7 min vs. 209.3 min).

It is clear that the *real* tested battery and the *simulated* DUALFOIL battery behave differently. The former exhibits much weaker nonlinearity than the latter. For batteries whose behavior is similar to that of the DUALFOIL battery, our lifetime predictions are of significant practical value. Otherwise, the results presented in this section should be treated as a demonstration of the high quality of our model with respect to variations in β – the parameter quantifying battery nonlinearity.

V. Model Application

In this section we provide details of the lifetime computation process. The equality (13) relates the lifetime L to the discharge history described by N staircase steps in the interval $[0, L]$. Given a load profile, we do not know L in

advance: it must be computed.

In general, we are given a profile with an arbitrary number of steps, say n. The battery failure occurs during some step $u = N - 1 \leq n - 1$, i.e., $L = t_N \in [t_u, t_{u+1}]$. Since a profile can contain rest periods, early failures may be masked after recovery. It is necessary to find the *earliest* failing step. Therefore, we consider load profile steps $\{0, 1, ..., u, ..., n-2, n-1\}$ in *increasing* order. Lifetime $L \in [t_u, t_{u+1}]$ is equal to the root x_0 of the following function $f(x)$:

$$f(x_0) = \alpha - \sum_{k=0}^{u-1} I_k F(x_0, t_k, t_{k+1}, \beta) - I_u F(x_0, t_u, x_0, \beta) = 0. \tag{17}$$

It is not necessary to search for a root in every step, i.e. some of them can be omitted. To determine whether some step u is guaranteed not to be failing, we need to examine the behavior of each term in (17) as x grows from t_u to t_{u+1}.

It is clear that only $F(x, t_k, t_{k+1}, \beta)$ and $F(x, t_u, x, \beta)$ are changing with respect to x. Recall that

$$F(x, t_k, t_{k+1}, \beta) = t_{k+1} - t_k + 2\sum_{m=1}^{\infty} \frac{e^{-\beta^2 m^2 (x - t_{k+1})} - e^{-\beta^2 m^2 (x - t_k)}}{\beta^2 m^2}. \tag{18}$$

It is straightforward to verify that $F(x, t_k, t_{k+1}, \beta)$ decreases as x grows. Therefore, the value of the sum $\sum_{k=0}^{u-1} I_k F(x, t_k, t_{k+1}, \beta)$ is *maximal* at the smallest $x = t_u$:

$$\sum_{k=0}^{u-1} I_k F(x, t_k, t_{k+1}, \beta) \leq \sum_{k=0}^{u-1} I_k F(t_u, t_k, t_{k+1}, \beta). \tag{19}$$

Similarly, one can see that

$$F(x, t_u, x, \beta) = x - t_u + 2\sum_{m=1}^{\infty} \frac{1 - e^{-\beta^2 m^2 (x - t_u)}}{\beta^2 m^2} \tag{20}$$

increases as x grows. Therefore, the term $I_u F(x, t_u, x, \beta)$ is *maximal* at the largest $x = t_{u+1}$:

$$F(x, t_u, x, \beta) \leq F(t_{u+1}, t_u, t_{u+1}, \beta). \tag{21}$$

Given relationships (19) and (21), we can state a sufficient condition for $L \notin [t_u, t_{u+1}]$:

$$\sum_{k=0}^{u-1} I_k F(t_u, t_k, t_{k+1}, \beta) + I_u F(t_{u+1}, t_u, t_{u+1}, \beta) \leq \alpha \Rightarrow L \notin [t_u, t_{u+1}]. \tag{22}$$

Thus, a given step u can be omitted by the root searching procedure, if inequality (22) holds; otherwise, we attempt to solve equation (17) within $[t_u, t_{u+1}]$. If the root is detected, it is returned as the estimated lifetime L. Otherwise, we proceed to the next step in the load profile.

The lifetime computation procedure is summarized in Figure 5. The load profile is described by the ordered sets $S_I = (I_0, I_1, ..., I_{n-1})$ and $S_t = (t_0, t_1, ..., t_{n-1})$. The finish time t_n of the last load is also specified. The procedure examines each step u, starting from $u = 0$, and checks condition (22). If this condition is not satisfied, the root searching procedure $Root(\cdot)$ is called. As arguments, it takes the function $f(x)$ itself and the boundaries of the search interval. If the root is detected, it is returned as the lifetime L in question. Otherwise, the next step $(u+1)$ is considered. Once all but the last steps are considered, the procedure computes the upper bound t_n^*. Note that the lower bound of $F(L, t_k, t_{k+1}, \beta) = t_{k+1} - t_k$ for all k; therefore, L must be less than $t_n^* = t_{n-1} + \frac{\alpha - \sum_{k=0}^{n-2} I_k (t_{k+1} - t_k)}{I_{n-1}}$. Procedure $Root(\cdot)$ takes $min\{t_n, t_n^*\}$ as the upper bound on the root value. If the battery survives all n steps, $L =$ **NULL** is returned.[1]

ComputeLifetime $(S_I, S_t, t_n, \alpha, \beta)$
  $L =$ **NULL**
  $u = 0$
  WHILE $u \leq n - 2$
    IF $\alpha < \sum_{k=0}^{u-1} I_k F(t_u, t_k, t_{k+1}, \beta) + I_u F(t_{u+1}, t_u, t_{u+1}, \beta)$
      $f(x) = \alpha - \sum_{k=0}^{u-1} I_k F(x, t_k, t_{k+1}, \beta) - I_u F(x, t_u, x, \beta)$
      $L = Root(f(x), t_u, t_{u+1})$
      IF $L \neq$ **NULL**
        RETURN L
    $u = u + 1$
  $t_n^* = t_{n-1} + \left[\alpha - \sum_{k=0}^{n-2} I_k (t_{k+1} - t_k)\right] / I_{n-1}$
  $f(x) = \alpha - \sum_{k=0}^{n-2} I_k F(x, t_k, t_{k+1}, \beta) - I_{n-1} F(x, t_{n-1}, x, \beta)$
  $L = Root(f(x), t_{n-1}, min\{t_n, t_n^*\})$
  RETURN L

Fig. 5. Lifetime Computation Procedure.

The computational complexity of $ComputeLifetime(\cdot)$ is dominated by the complexity of the **WHILE** loop. This loop is executed $O(n)$ times, and at each iteration the procedure computes $\sum_{k=0}^{u-1} I_k F(t_u, t_k, t_{k+1}, \beta)$ and the root of equation (17), if necessary. A brute-force implementation of $Root(\cdot)$ can be as follows. Let δ denote the time-axis resolution (i.e. the smallest unit used to specify timing), and let Δ denote the length of the longest time interval in the n-step load approximation. Starting from $x = t_u$, the next value of the argument is $x = x + \delta$; thus, the number of arguments examined is at most Δ/δ. For each x within $[t_u, t_{u+1}]$, one needs to check whether $\sum_{k=0}^{u-1} I_k F(x, t_k, t_{k+1}, \beta) + I_u F(x, t_u, x, \beta)$ exceeds α; this takes $O(n)$ time. Therefore, the complexity of lifetime computations is $O(n^2 \frac{\Delta}{\delta})$. Note that the values of n, Δ and δ can be controlled by the user. Increasing n, for example, improves load approximation and, consequently, the accuracy of lifetime predictions; however, the computational complexity increasee as well. Permitting this tradeoff is another advantageous feature of the proposed model.

VI. Conclusion

We described an analytical battery model that not only allows a designer to predict the battery time-to-failure for a given load, but also provides a cost metric for an optimization algorithm that aims at maximization of the battery lifetime. Our model also allows for a tradeoff between the accuracy and the amount of computation performed.

[1] Note that if $t_n \geq t_n^*$, then L is guaranteed to exist.

The functional form of the proposed model is derived based on physical principles, and its two coefficients are estimated based on the results of several constant-current tests. The model predictions were compared with the simulation data under the constant and variable discharge conditions (these 44 tests resulted in the lifetimes ranging from 1/2 hour to 200 hours). For all of the 22 constant load tests, the prediction error was within 10%, and for all of the 22 variable load tests, the prediction error was within 5%.

In addition, we verified our model against actual measurements taken on a real lithium-ion battery used in a pocket computer. For 12 constant-load tests performed, the maximum error of lifetime predictions was 4%. For 21 variable-load tests performed, the accuracy of our lifetime estimates was within 1%.

VII. Acknowledgments

This work was carried out at the National Science Foundation's State/Industry/University Cooperative Research Centers' (NSF-S/IUCRC) Center for Low Power Electronics (CLPE) and Compaq Western Research Laboratory (WRL). CLPE is supported by the NSF (Grant EEC-9523338), the State of Arizona, and a consortium of companies from the microelectronics industry (visit the CLPE web site http://clpe.ece.arizona.edu).

VIII. Appendix

We are given the following system of two partial differential equations, two boundary conditions, and one initial condition:

$$-J(x,t) = D\frac{\partial C(x,t)}{\partial x}, \tag{23}$$

$$\frac{\partial C(x,t)}{\partial t} = D\frac{\partial^2 C(x,t)}{\partial x^2}, \tag{24}$$

$$-J(0,t) = \frac{i(t)}{\nu FA}, \tag{25}$$

$$J(w,t) = 0, \tag{26}$$

$$C(x,0) = C^*, \ \forall\ x. \tag{27}$$

After applying the Laplace transformation $C(x,t) \rightarrow \bar{C}(x,s)$, we obtain

$$\bar{C}(x,s) = \frac{C^*}{s} + P\ e^{-x\sqrt{\frac{s}{D}}} + Q\ e^{x\sqrt{\frac{s}{D}}}, \tag{28}$$

$$\frac{d\bar{C}(x,s)}{dx} = -\sqrt{\frac{s}{D}}\Big(P\ e^{-x\sqrt{\frac{s}{D}}} - Q\ e^{x\sqrt{\frac{s}{D}}}\Big). \tag{29}$$

We are only interested in the concentration at the electrode surface ($x = 0$). The Laplace transformation $i(t) \rightarrow \bar{i}(s)$ and application of the boundary conditions for $x = 0$ and $x = w$ yield the following system of equations:

$$\bar{C}(0,s) = \frac{C^*}{s} + P + Q, \tag{30}$$

$$\frac{\bar{i}(s)}{\nu FAD} = -\sqrt{\frac{s}{D}}\Big(P - Q\Big), \tag{31}$$

$$0 = -\sqrt{\frac{s}{D}}\Big(P\ e^{-w\sqrt{\frac{s}{D}}} - Q\ e^{w\sqrt{\frac{s}{D}}}\Big). \tag{32}$$

The solution of this system is as follows:

$$\bar{C}(0,s) = \frac{C^*}{s} - \frac{\bar{i}(s)}{\nu FAD}\frac{\coth(w\sqrt{\frac{s}{D}})}{\sqrt{\frac{s}{D}}}. \tag{33}$$

We utilize the property that multiplication in the s-domain corresponds to convolution in the time-domain; after performing the inverse Laplace transformation of equation (33), we obtain [20]:

$$C(0,t) = C^* - \frac{i(t)}{\nu FAD} * \sqrt{\frac{D}{\pi t}}\sum_{m=-\infty}^{\infty} e^{-\frac{w^2m^2}{Dt}}, \tag{34}$$

$$1 - \frac{C(0,t)}{C^*} = \frac{1}{\nu FA\sqrt{\pi D}C^*}\int_0^t \frac{i(\tau)}{\sqrt{t-\tau}}\sum_{m=-\infty}^{\infty} e^{-\frac{w^2m^2}{D(t-\tau)}}\ d\tau. \tag{35}$$

Next, we use the following identity from the theory of theta functions [21]:

$$\sum_{m=-\infty}^{\infty} e^{-ym^2} = \sqrt{\frac{\pi}{y}}\sum_{m=-\infty}^{\infty} e^{-\frac{\pi^2m^2}{y}}\ ,\ Re(y) > 0. \tag{36}$$

In (36), let $y = \frac{w^2}{D(t-\tau)} > 0$. Then,

$$1 - \frac{C(0,t)}{C^*} = \frac{1}{\nu FAwC^*}\int_0^t i(\tau)\Big[1 + 2\sum_{m=1}^{\infty} e^{-\frac{\pi^2D(t-\tau)m^2}{w^2}}\Big]\ d\tau. \tag{37}$$

For $\tau \in [0,t]$, the exponential series is uniformly convergent[2], and we can integrate the series term by term. Then,

$$1 - \frac{C(0,t)}{C^*} = \frac{1}{\nu FAwC^*}\Big[\int_0^t i(\tau)\ d\tau + 2\sum_{m=1}^{\infty}\int_0^t i(\tau)\ e^{-\frac{\pi^2D(t-\tau)m^2}{w^2}}\ d\tau\Big]. \tag{38}$$

References

[1] D. Linden, *Handbook of Batteries*, McGraw-Hill, New York, 1995.

[2] T. Martin, *Balancing Batteries, Power, and Performance: System Issues in CPU Speed-Setting for Mobile Computing*, PhD Dissertation, Carnegie Melon University, 1999.

[3] M. Pedram and Q. Wu, "Design considerations for battery-powered electronics," *Proc. DAC*, 1999.

[4] T. Simunic, L. Benini, and G. De Micheli, "Energy-efficient design of battery-powered embedded systems," *IEEE Trans. VLSI Syst.*, February 2001.

[5] M. Doyle, T. Fuller, and J. Newman, "Modeling of galvanostatic charge and discharge of the lithium/polymer/insertion cell," *J. Electrochem. Soc.*, vol. 140, no. 6, 1993.

[6] T. Fuller, M. Doyle, and J. Newman, "Simulation and optimization of the dual lithium ion insertion cell," *J. Appl. Electrochem.*, vol. 141, no. 1, 1994.

[7] S. Gold, "A PSPICE macromodel for lithium-ion batteries," *Proc. Battery Conf.*, 1997.

[2] Note that $\tau \in [0,t] \Rightarrow \frac{\pi^2D(t-\tau)}{w^2} > 0 \Rightarrow\ e^{-\frac{\pi^2D(t-\tau)m^2}{w^2}} < 1$ for all $m \geq 1$. Since $|\ e^{-\frac{\pi^2D(t-\tau)(n+m)^2}{w^2}} - e^{-\frac{\pi^2D(t-\tau)m^2}{w^2}}| < 1$ for all $n, m \geq 1$, the Cauchy criterion for convergence holds; therefore, the series is uniformly convergent.

[8] L. Benini, G. Castelli, A. Macii, E. Macii, M. Poncino, and R. Scarsi, "A discrete-time battery model for high-level power estimation," *Proc. Design Automation Test Europe*, 2000.
[9] D. Panigrahi, C. Chiasserini, S. Dey, R. Rao, A. Raghunathan, and K. Lahiri, "Battery life estimation of mobile embedded systems," *Proc. VLSI Design*, 2001.
[10] M. Doyle and J. Newman, "Modeling the performance of rechargeable lithium-based cells: design correlations for limiting cases," *J. Power Sources*, vol. 54, 1995.
[11] K. Syracuse and W. Clark, "A statistical approach to domain performance modeling for oxyhalide primary lithium batteries," *Proc. Battery Conf.*, 1997.
[12] A. Bard and L. Faulkner, *Electrochemical Methods*, Wiley, New York, 1980.
[13] I. Gradshteyn and I. Ryzhik, *Table of Integrals, Series, and Products*, Academic Press, New York, 1965.
[14] M. Viredaz and D. A. Wallach, "Power evaluation of a handheld computer: a case study," *Compaq WRL Research Report 2001/1*, May 2001.
[15] P. Arora, M. Doyle, A. Gozdz, R. White, and J. Newman, "Comparison between computer simulations and experimental data for high-rate discharges of plastic lithium-ion batteries," *J. Power Sources*, vol. 88, 2000.
[16] IBM, *Microdrives*, Product Specification, 2001.
[17] Lucent, *Orinoco WaveLAN*, Product Specification, 2001.
[18] K. Farkas, J. Flinn, G. Back, D. Grunwald, and J. Anderson, "Quantifying the energy consumption of a pocket computer and a Java Virtual Machine," *Compaq WRL Research Report 2000/5*, June 2000.
[19] D. A. Wallach, "Interpreting the battery lifetime of the Itsy version 2.4," *Compaq WRL Technical Note TN-61*, December 2001.
[20] G. Roberts and H. Kaufman, *Table of Laplace Transforms*, Saunders, Philadelphia, 1966.
[21] R. Bellman, *A Brief Introduction to Theta Functions*, Holt, Rinehart and Winston, New York, 1961.